Characterisation of topical film-forming systems using atomic force microscopy and Raman micro-spectroscopy

Hazel Garvie-Cook[1,2], Kit Frederiksen[2,3], Karsten Petersson[3], Richard Guy[2], Sergey Gordeev[1*]

1. Department of Physics, University of Bath, Bath, UK
2. Department of Pharmacy & Pharmacology, University of Bath, Bath, UK
3. LEO Pharma A/S, DK-250 Ballerup, Denmark

[*] All correspondence to: Sergey Gordeev, Department of Physics, University of Bath, Claverton Down, Bath, BA2 7AY

Tel number: +44 (0) 1225 385154, Email address: s.gordeev@bath.ac.uk

Abstract

Polymeric film-forming systems for dermal drug delivery represent an advantageous alternative to more conventional topically applied formulations. Their mechanical properties and homogeneity can be characterised with atomic force microscopy (AFM), using both imaging and nanoindentation modes, and Raman micro-spectroscopy mapping. Film-forming polymers, with and without a plasticizer and/or betamethasone 17-valerate (a representative topical drug), were dissolved in absolute ethanol. Polymeric films were then cast on glass slides and examined in ambient air using AFM imaging and Raman micro-spectroscopy. Using nanoindentation, the elastic moduli of various films were determined and found to decrease with increasing plasticizer content. Films with 20% w/w plasticizer had elastic moduli close to that of skin. AFM images showed little difference in the topography of the films on incorporation of plasticizer. Raman micro-spectroscopy maps of the surface of the polymeric films, with a spatial resolution of approximately 1 μm, revealed homogenous distributions of plasticizer and drug within the films.

Keywords

Atomic force microscopy · Raman micro-spectroscopy · Nanoindentation · Dermal drug delivery · Polymeric film-forming systems

Abbreviations

AFM, atomic force microscopy. BMV, betamethasone valerate. EBID, electron beam induced deposition. FFS, film-forming systems. SEM, scanning electron microscopy. TEC , triethyl citrate.

1. Introduction

In situ, polymeric film-forming systems (FFS) represent a potentially advantageous approach to dermal drug delivery compared to conventional topical dosage forms. FFS are composed of a film-forming polymer, with or without a plasticiser, and a drug substance all dissolved in a volatile solvent. Upon application of the FFS to the skin, the solvent evaporates, and a thin, transparent, flexible and cosmetically elegant film is formed [1]. The FFS aims to efficiently deliver the required amount of therapeutic agent to the target site in the skin over an extended period of time. Ideally, FFS should have short drying times and good rub-off resistance (or substantivity) relative to typical semisolid preparations.

In terms of drug delivery, the use of polymeric FFS in tablet coatings is well documented [2]. FFS are also used in surgery, for example, to help in the closing of incisions [3, 4] and in the pre-operative preparation of skin at the incision site [5]. A systematic review of polymeric FFS for (trans)dermal drug delivery was recently published [1].

The FFS considered here were based on either a hydrophilic (Klucel) or a hydrophobic (Eudragit) polymer. These polymers, known pharmaceutical excipients [6, 7], were selected after screening as representative hydrophilic and hydrophobic examples. Screening was based on the polymers' solubility in ethanol, their ability to form complete, transparent films of low stickiness, and an ability to sustain BMV release over 72 hours [8]. Eudragit and Klucel are used in tablet coatings, and the latter is also employed in topical formations, including gels and lotions [9]. Ethanol was selected as a pharmaceutically acceptable solvent suitable for BMV. The plasticiser, triethyl citrate (TEC), which is commonly used in film coatings of tablets, was included to improve the mechanical properties (especially the flexibility [10]) of, and the drug release behaviour [11] from, the resulting films [1, 12, 13]. Film flexibility on the surface of skin is important to maintain intimate contact and to ensure that the area, across which drug transport occurs, remains constant. This is essential to achieve the desired therapeutic benefit and to guarantee patient safety [14]. A range of FFS vehicles, optimised for fast-drying, non-tackiness and invisibility on the skin, have been formulated and tested.

AFM can provide both topographical and mechanical information about polymeric films to support formulation development and to optimise FFS composition to match the mechanical properties of the films to those of skin. AFM can generate a nanoscale image of a film's homogeneity and roughness and is an ideal technique with which to study biological samples; measurements can be made in ambient/physiological conditions, and require no special treatment prior to measurement (such as staining or coating, which could damage the sample).

Furthermore, the sensitivity of the AFM cantilever to small forces can be utilized in nanoindentation, a valuable tool for the determination of local mechanical properties (such as hardness and elastic modulus) of biological samples [15]. Nanoindentation has previously been used to characterise pharmaceutical solids, such as sucrose [16] and acetaminophen [17], and to determine the effect of a topical product on skin (nano)biomechanics [18]. Nanoindentation measurements of films for dermal drug delivery give information on mechanical differences caused by the incorporation of plasticizers. These measurements enable the elastic properties of the films to be matched to those of skin.

Raman spectra of the polymeric films reveal information about their chemical composition. Chemical maps of the films, based on a collection of Raman spectra taken with spatial separations of 1 μm, provide a measure of the chemical homogeneity of the films. The intensity of Raman scattering is directly proportional to the concentration of the substance from which it originates [19]. In the pharmaceutical industry, this technique gives information on constituent distribution and concentration in tablets [20-22], transdermal tapes [23], film-forming emulsions for dermal drug delivery [24], and nasal spray formulations [25]. Techniques based on Raman scattering can also be used to track the permeation of topically applied compounds through the skin [26, 27].

In this work, polymeric films for dermal drug delivery were imaged at the nanoscale using AFM. To determine the effect of the incorporation of a plasticiser (TEC) on the elastic properties of the film, AFM nanoindentation measurements were performed on polymeric films formed from FFS of varying compositions. Indentation data were analysed using both the classical elastic (Hertz) model and a

model, developed in this work, for viscous-elastic-plastic deformation with a spherical indenter. AFM images of the films showed a smooth surface with a roughness below 4nm for Eudragit films and larger scale roughness in Klucel films. The films appeared mechanically homogenous. Nanoindentation revealed that the addition of plasticizer caused a reduction in the elastic moduli of the films. Films with 20% w/w TEC had elastic moduli similar to the elastic modulus of skin [28]. The addition of a representative topical drug, betamethasone valerate (BMV), had no significant effect on the mechanical properties of the films. Raman mapping showed that plasticizer and BMV were distributed homogeneously across the mapped area.

2. Materials and Methods

2.1 Materials

Eudragit®RS (ammonio methacrylate copolymer type B) was generously donated by Evonik Röhm GmbH (Darmstadt, Germany) and Klucel™ LF (hydroxypropyl cellulose) by Azelis (Lyngby, Denmark). TEC and BMV were from LEO Pharma A/S, (Ballerup, Denmark).

2.2 Preparation of polymeric FFS

FFS were prepared by combining polymer and absolute ethanol and plasticizer, if used. A 10% w/w solution of TEC in absolute ethanol was first prepared by stirring for two hours to ensure complete dissolution. The plasticizer stock was then mixed with the appropriate amount of polymer, also dissolved in ethanol, the concentration used being dependent upon the FFS desired. The film-forming solution was stirred overnight and a clear solution was obtained. The representative topical drug (BMV) was then dissolved in the FFS at a concentration of 1.2% w/w (corresponding to 1% betamethasone). Table I summarizes the FFS compositions investigated in this work.

Table 1 A summary of the compositions of the FFS tested.

Formulation	Polymer	TEC	Absolute ethanol	Water
15% Eudragit without plasticizer	15	0	80	5
15% Eudragit with 20% TEC	15	3	77	5
15% Eudragit with 40% TEC	15	6	74	5
5% Klucel without plasticizer	5	0	95	0
5% Klucel with 20% TEC	5	1	94	0
5% Klucel with 40% TEC	5	2	93	0

Content is given in mass fractions %(w/w). Percentages of TEC correspond to the percentage of dry polymer weight.

For AFM imaging, nanoindentation and Raman mapping, the FFS were cast uniformly onto clean glass slides, using a micropipette to dispense the solution and spread it out over the required area. The coated slides were maintained overnight at approximately 30°C to mimic the temperature of the skin surface. Formed films had thicknesses of approximately 10 μm.

2.3 Raman microscopy

Raman spectroscopic measurements were performed using an inVia Raman microscope (Renishaw, Wotton-under-Edge, UK). The excitation source was a laser operating at a wavelength of 532 nm. To determine the characteristic peaks of each component of the films, Raman spectra of Eudragit, Klucel, TEC and BMV were initially obtained using 10% of the maximum laser power available, approximately 80 mW. Peaks observed in the Raman spectra of TEC and BMV, that were distinct from peaks observed in the spectra of the polymers, were used in the mapping to determine the spatial distribution of these molecules.

Raman mapping was performed over areas of approximately 17 x 23 μm^2 on both Eudragit and Klucel films containing 20% TEC and 1.2% BMV. To obtain a high resolution map of the polymeric films to

complement the AFM images, the excitation beam was passed through a pinhole to decrease the volume of interaction. The Raman signal obtained in this way originated from an area of approximately 1 x 1 μm^2, which then corresponded to the area of each pixel in the chemical maps. Mapping was performed with the maximum laser power available (80 mW) at which no damage to the sample was observed.

Wire 3.4 software (Renishaw) was used to analyse the Raman spectra. Spectral parameters were defined and fitted to specific scattering peaks for TEC and BMV. The intensities of the TEC and BMV peaks at each position then allowed the chemical composition of the film to be mapped.

2.4 Atomic Force Microscopy

AFM experiments were performed using a Multimode Scanning Probe Microscope (Veeco, Plainview, NY) with a Nanoscope IIIA controller and Nanoscope software (Version 7.341).

2.4.1 Imaging

Images were obtained in tapping mode under ambient conditions. 'All in One' AFM probes (AlOAl, Budget Sensors, Sofia, Bulgaria), with nominal spring constants between 0.2 and 40 N/m and resonance frequencies between 15 and 350 kHz, were used for both imaging and nanoindentation. Images were analysed using Nanoscope Analysis (Version 1.3, Bruker, Billerica, MA).

2.4.2 Nanoindentation

The spring constant of each AFM probe used in these experiments was accurately determined according to published methodology [29].

The shape and radius of curvature of the AFM probe tips used for nanoindentation were evaluated by scanning electron microscopy (SEM) (6301F, JEOL, Tokyo, Japan). Probes with tips of rounded appearance were selected. By increasing the radius of curvature of the probe tip, the resolution of indentation measurements decreases but the tip is less likely to plastically deform the sample under low loads. If the probes were not spherical or did not have a large enough radius, electron beam induced deposition (EBID) [30] was used to produce rounded tips from standard AFM probes. As the maximum depth of indentation was below the radius of curvature of the probes selected, between 27 and 80 nm, the shape of the indenter could be considered spherical.

All indentation measurements were performed in contact mode. Parameters such as the approach rate and surface delay were specified prior to indentation. The deflection of the AFM cantilever, as it was brought into contact with the sample and caused deformation, was recorded as a function of its displacement in the vertical direction from its initial position. The elastic modulus of the sample was assessed from these data using Hertz [31] and Oyen & Cook [32] models.

3. Results

3.1 Raman spectra of film constituents

Raman spectra of the individual constituents of the films were first recorded (Figure 1), to determine characteristic peaks by which they could be identified.

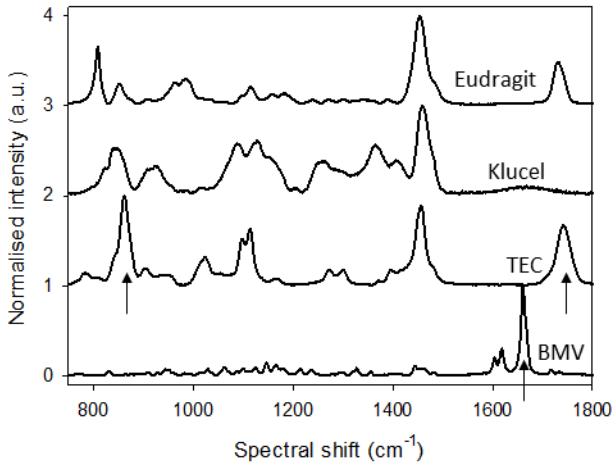

Figure 1. Raman spectra of the constituents of polymeric films: Eudragit, Klucel, TEC and BMV. Spectra are normalised according to the maximum intensity. Arrows indicate the position of characteristic peaks for TEC and BMV.

Obvious characteristic peaks for BMV and TEC were identified at 1670 cm^{-1} and 1734 cm^{-1}, respectively. The peak for BMV was used to monitor the drug in both polymer films; however, while the 1734 cm^{-1} peak for TEC could be clearly distinguished in the Klucel films, it overlapped significantly with a Raman signal from Eudragit. In these films, therefore, TEC was mapped using its unique peak intensity at 857 cm^{-1}.

3.2 Raman chemical mapping

Mapping was performed at a high spatial resolution to compare with AFM images. The intensities of the characteristic peaks of TEC and BMV as a function of position along a representative line in the Raman maps of films of (a) Eudragit and (b) Klucel, both with 20% TEC and 1.2% BMV, are shown in Figure 2. The polymer was assumed to be evenly distributed throughout the film and its Raman signal was therefore used to normalise those from TEC and BMV. For Eudragit with 20% TEC and 1.2% BMV, the concentrations of plasticiser and drug varied by less than 4%.

Mapping of the Klucel film with 20% TEC and 1.2% BMV was then performed, with exactly the same result. That is, the intensities of the characteristic peaks of TEC and BMV as a function of position along a representative line showed relatively small variation (in this case, to no more than 4%).

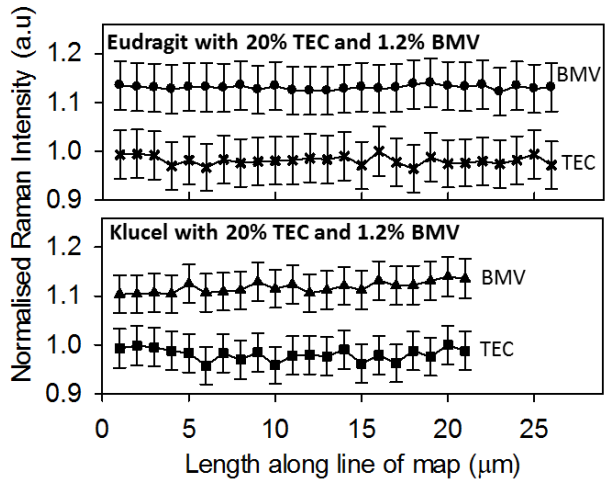

Figure 2. Representative Raman line scans of the distribution of BMV and TEC in Eudragit and Klucel films with 20% TEC and 1.2% BMV. Line scans are taken along one line of a chemical map of

each sample. The maps were obtained from the intensities of characteristic BMV and TEC Raman peaks and were recorded every 1 x 1 μm^2.

3.3 AFM images

AFM images of the topography of the films deposited on glass slides were acquired. Tapping mode images were taken over scan areas of 4 x 4 μm^2 for all film compositions and two examples are shown in Figure 3. Tapping mode imaging was used, as opposed to contact mode, to minimise damage to the softer, plasticized films. Unplasticized Eudragit films (Figure 3(a)) show relatively small structural features, with heights just below 4 nm (Figure 3(c)), over the surface of the film. Klucel without plasticizer shows larger scale structures and a greater roughness (Figure 3(b)) of approximately 20 nm (Figure 3(c)). Addition of plasticiser to Eudragit films smoothed the topography further whereas the opposite occurs when plasticizer is introduced at 40% into Klucel films (Figure 3(c)). This effect on roughness could be attributed to the plasticizer in the polymer network providing "gap fillers", which result in smoother Eudragit films [33]. The effect of plasticizer on roughness may be different in Klucel films due to the much larger molecular weight of Klucel (95,000 Da), relative to the plasticizer (276 Da), and compared to Eudragit (32,000 Da). There were no obvious signs of component separation in the AFM images of any film either with or without plasticizer, suggesting that TEC and BMV were distributed evenly throughout the film.

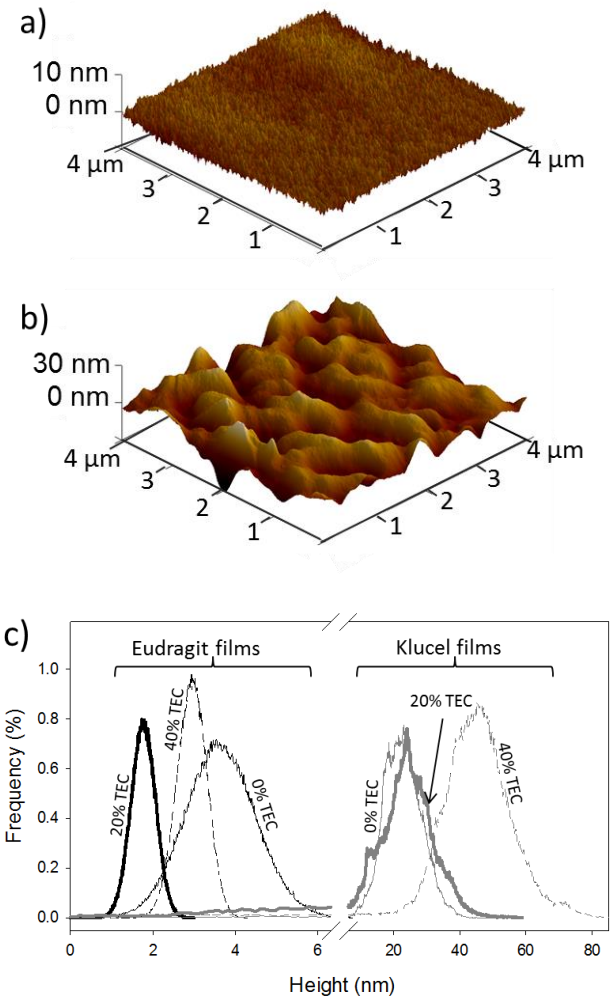

Figure 3. Pseudo 3D AFM images of polymeric films without plasticiser, cast onto glass microscope slides, at scan sizes of 4x4 μm^2: (a) Eudragit, and (b) Klucel. Histograms of feature height frequency are in (c), for polymers incorporating 0%, 20% and 40% TEC plasticizer.

3.4 Nanoindentation

During AFM nanoindentation, a minimum of eight indents were carried out on each sample. Indents were separated by at least 500 nm along the sample surface to ensure that each new indent would deform a previously unaffected area of the film. The approach and retract data were taken in one measurement cycle and the approach and retract rates of the probe were either 4 nm/s or 16 nm/s as specified. For some measurements, a hold of 10 seconds was introduced at the maximum vertical displacement of the probe before its retraction.

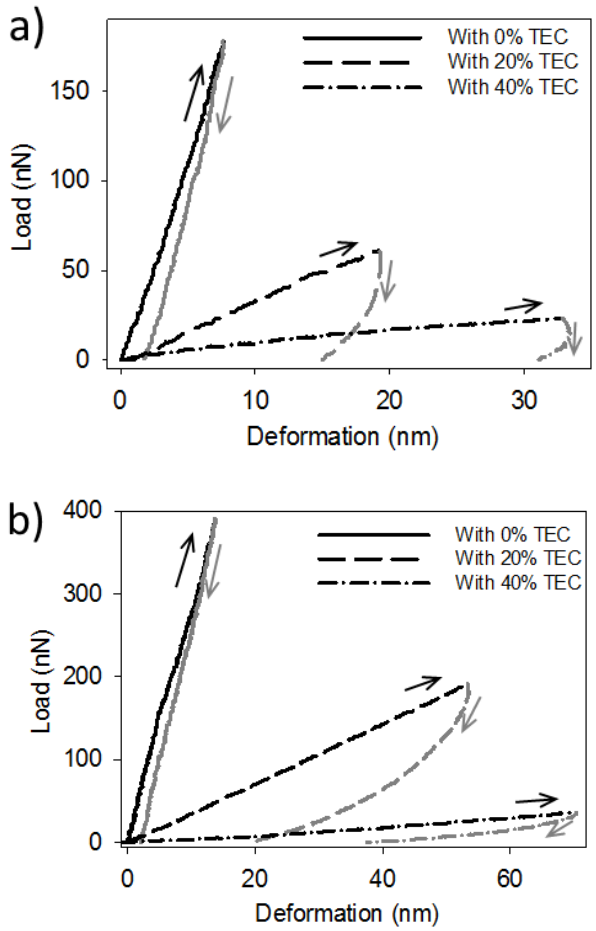

Figure 4. Load as a function of deformation during indentation: (a) Eudragit with 0, 20 and 40% TEC, and (b) Klucel with 0, 20 and 40% TEC.

The load applied to the sample by the probe tip was calculated from the cantilever's deflection and its spring constant. The deformation of a polymeric film (h) at a given deflection (D) is:

$$h = \Delta z(D) - \Delta z_C(D) \qquad (1)$$

where $\Delta z(D)$ and $\Delta z_C(D)$ are vertical displacements of the AFM probe, relative to the points of first contact, for the polymer film and for a non-deformable calibration sample (glass), respectively.

The variation of deformation with load on the polymeric films reveals the indentation behaviour of the sample and allows selection of a model to fit the data and to extract the corresponding elastic modulus. Load-deformation behaviours of all samples are shown in Figure 4, which clearly reveal the impact of the plasticizer. The load-deformation result for Eudragit without plasticizer shows the

highest load needed for the least deformation. For the film containing 20% TEC, application of a lower load produces more deformation showing that the sample is softer. The change is amplified further when 40% TEC is incorporated. Similar behaviour was observed for the Klucel films.

Figure 4 also reveals that the deformation of all samples is both elastic and plastic. There is hysteresis between the approach and the retract curves, meaning that some plastic deformation has occurred. When the force from the AFM probe tip is removed and the cantilever returns to its initial deflection, a residual deformation is present as the sample has been permanently deformed.

Viscous deformation was investigated by varying approach rate and surface delay. The approach rate is the speed at which the probe is pushed into the sample. The same speed is used to retract the probe tip from the sample. A surface delay is used to examine the creep of the probe when it indents the sample. To observe this creep, the probe tip is held at the AFM cantilever's maximum vertical displacement, corresponding to the greatest load on the sample. If the sample shows viscous behaviour, the probe will sink further into the sample during this holding period even though the cantilever is being held at a fixed vertical position. The effects of approach rate and surface delay on load as a function of deformation during AFM nanoindentation are shown in Figures 5 and 6.

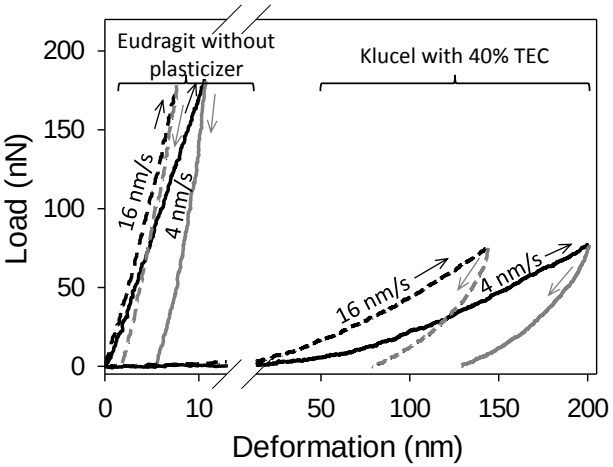

Figure 5 Load as a function of deformation during indentation of Eudragit without plasticizer and Klucel with 40% TEC at approach rates of 4 nm/s (solid lines) and 16 nm/s (dashed lines).

Less hysteresis between the approach and retract curves was observed at a higher approach rate (Figure 5), which allows less time for viscous relaxation. When approaching at a high rate, the sample presents a greater resistance to deformation and the apparent stiffness is higher.

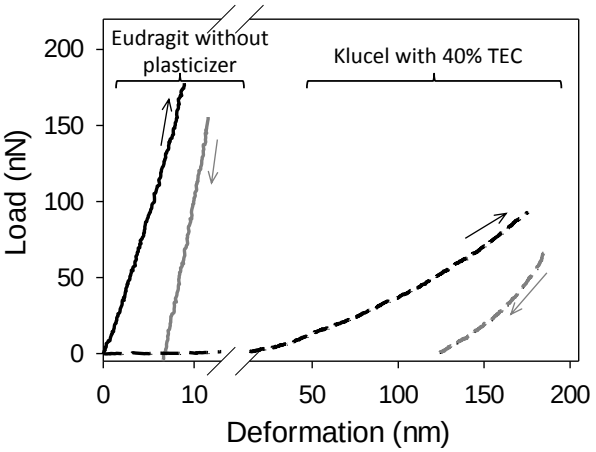

Figure 6 Load as a function of deformation during indentation of Eudragit without plasticizer (solid lines) and Klucel with 40% TEC (dashed lines). A surface delay of 10 s and an approach rate of 16 nm/s were used in these measurements.

The impact of viscosity is also illustrated in Figure 6. During the hold period, while the cantilever is maintained at its maximum displacement, the probe sinks further into the sample and the deflection of the cantilever decreases. This, in turn, results in a decrease of the load on the sample. In the case of Eudragit without plasticizer, the load has decreased to 87% of its original value before the hold period; for Klucel with 40% TEC, the corresponding figure is 71%. This result is consistent with the more viscous nature of the sample containing TEC plasticizer.

4. Discussion

4.1 Raman chemical mapping

To judge the significance of the variability observed in Raman maps of TEC and BMV within Eudragit films (Figure 2), variation in the spectral intensity of a characteristic polymer peak was determined after different methods of background subtraction. The changes in intensity could therefore be considered as error. It was found that, in the case of the Eudragit film, the polymer signal varied by 5%; that is, greater than the variations observed in the TEC and BMV signals. It follows that, within the precision of the measurements made, it can be concluded that BMV and TEC are distributed evenly over the mapped area.

The variability of TEC and BMV across the mapped areas of Klucel films was identical to that of the polymer signal variability. Again, therefore, it was deduced that TEC and BMV were distributed evenly over the mapped area, consistent with the topographical information from the AFM images (i.e., film homogeneity and no phase separation).

4.2 Determination of elastic modulus

The elastic modulus of the polymeric films at each indent was determined using two different models. The first, the most commonly used to interpret nanoindentation data, was the Hertz model, which approximates the indented sample as a linear elastic solid. The assumptions of the model are (i) the indenter is non-deformable, (ii) there are only elastic interactions between the probe tip and the sample, (iii) the sample is homogeneous, and (iv) the indentation is negligible compared to the sample thickness [34]. While the original model addressed the contact between two spheres, the theory is easily modified to obtain an expression for the load (P) on a planar sample contacted by a spherical indenter [35]:

$$P = (4/3) \times R^{1/2} \times E_r \times h^{3/2} \qquad (2)$$

where R is the radius of curvature of the spherical indenter and E_r is the reduced elastic modulus of the sample, from which the elastic modulus can be determined. The geometry of the indenter determines the power to which the deformation h is raised.

The Hertz model assumes elastic behaviour, i.e., no hysteresis in the load-deformation behaviour of the sample. In many cases, small deformations, much shallower than the thickness of the sample, can be assumed to be elastic.

The second (Oyen & Cook) model [32], designed for viscous-elastic-plastic behaviour, extracts the elastic modulus from the unloading/retract curves of samples. Viscous deformation is time-dependent so the model includes consideration of the time during indentation. In this model, the elastic, plastic and viscous deformations of the sample are represented by an elastic spring, a plastic deformation element and a damping element in series. This model was initially developed for conical indentation but has been modified for spherical indentation. As shown in Equation 2, for elastic deformation with

a spherical indenter, the load P is proportional to $h^{3/2}$. It can be assumed that viscous deformation for spherical indentation follows a power law with the same index as that for elastic deformation:

$$P_v = \mu \times (dh_v/dt)^{3/2} \quad (3)$$

where P_v is the load on the viscous damping element, μ is the damping coefficient, h_v is the displacement of the damping element and t is the time during indentation. It is usually assumed [32] that during unloading no additional plastic deformation of the sample occurs.

For the series model, the total load is the same in each element and the total displacement of the sample (h_{total}) is the sum of the displacements in each element:

$$h_{total} = h_e + h_v \quad (4)$$

Following the Oyen & Cook method [32], the load from the AFM probe was increased by approaching the tip to the sample at a constant rate, for a time τ_L until the maximum load P_{max} was reached. The tip was then held on the sample surface for a time τ_H at a constant vertical displacement. Finally, the probe was retracted at a constant rate for a time τ_U until the probe and the sample were no longer in contact. These loading conditions are shown in the inset to Figure 7.

From Equations 2, 3 and 4, an expression for the total deformation during the unloading portion of the indentation ($h^{UNLOAD}(t)$) is obtained:

$$h^{UNLOAD}(t) = (P_{max}/\tau_U)^{2/3} \times \Delta t^{2/3} \times \{k_Q^{-2/3} - [(3/5) \times \mu^{-2/3} \times \Delta t]\} + h_f \quad (5)$$

where $\Delta t = \tau_L + \tau_H + \tau_U - t$, t is the time of the measurement, μ is a damping coefficient, h_f is the deformation remaining after all force applied by the probe tip is removed, and $k_Q = (4/3) \times R^{1/2} \times E_r$.

Equation 5 may be simplified to

$$h^{UNLOAD}(t) = (a \times \Delta t^{2/3}) + (b \times \Delta t^{5/3}) + c \quad (6)$$

and fitted to the unloading data. From the derived parameter (a), the reduced modulus was then extracted. An example of the fit of this model to the experimental data is shown in Figure 7.

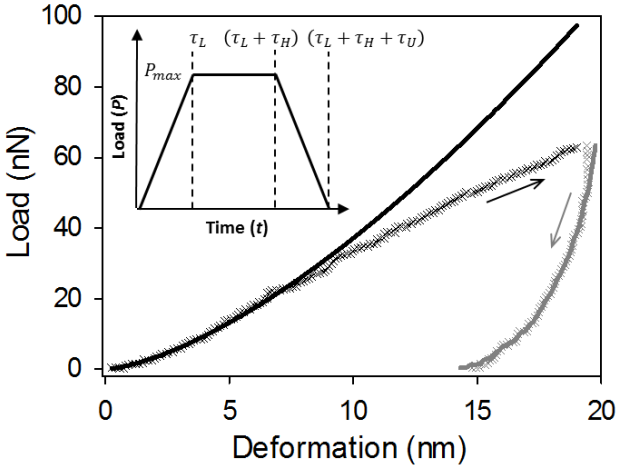

Figure 7. Fits of the Hertz and Oyen & Cook models (upper and lower solid lines, respectively) to the experimentally measured load as a function of deformation (crosses) during indentation of Eudragit with 20% TEC. The inset to the figure shows the AFM loading conditions employed in the experiment. Load is increased for a period τ_L until the maximum (P_{max}) is reached. The probe is then held at this position for a time τ_H. The probe is subsequently retracted at a constant rate over time τ_U. The experimental data in black were obtained during τ_L, those in grey were recorded over time τ_U. For the data presented in the main panel, τ_U=0.

The reduced modulus E_r, which takes into account the elastic modulus of the indenter and of the sample itself, was calculated using both models. Given that the indenter modulus (150 GPa for silicon [36] and 28 GPa for EBID [37]) was much greater than those of the samples tested (0.05-1.6 GPa), the elastic modulus (E) of the film can be approximated by:

$$E = E_r \times (1 - \nu^2) \quad (8)$$

where ν is its Poisson's ratio (0.495 for Eudragit and Klucel [38]).

Elastic moduli derived using the Oyen & Cook method are consistently higher than those obtained with the Hertz model (Figure 8). If the sample showed only elastic behaviour, the fit of the Hertz model to the loading curve would be significantly better than that shown in Figure 7, as less deformation would be occurring at a given load without plastic and viscous deformation taking place. Instead, the Hertz model overestimates the amount of elastic deformation during loading and, as a result, the calculated elastic modulus is an underestimation. The Oyen & Cook model takes into account viscous, elastic and plastic deformation of the sample and therefore more accurately determines the elastic modulus. Further, it was found that using different approach rates (4 and 16 nm/s), and a delay on the sample surface of up to 10 s, had no significant effect on the assessed elastic modulus for any film, demonstrating that the second model has successfully taken into account the differences in the viscous behaviour of the samples at different loading conditions.

The elastic moduli, calculated using the Hertz model and the modified Oyen & Cook model, of all the polymeric films examined, are in Figure 8. Elastic moduli decreased with increasing plasticizer content, as expected [2]. The elastic modulus of human skin, determined using a similar technique to that employed here, approximately 0.3 GPa [28], is lower than those of unplasticized Eudragit and Klucel films. It was found that 20% TEC had to be introduced into the polymers to bring their elastic moduli below that of skin and to ensure that the films will be flexible when applied topically and enable intimate and prolonged contact. It should be noted that too much plasticizer could cause polymer films to become tacky [1] and careful optimisation of a formulation is required to maximise both the mechanical and sensorial properties.

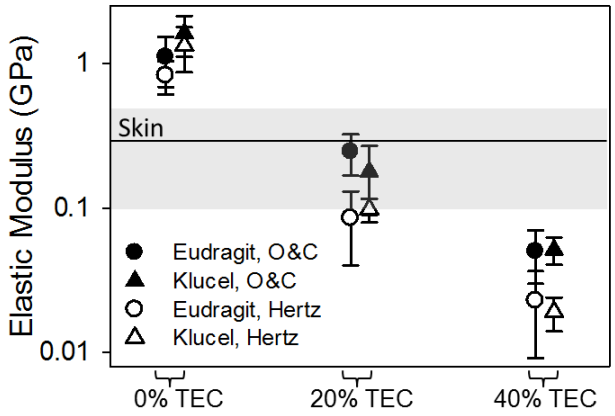

Figure 8 Elastic moduli of Eudragit and Klucel films without and with different amounts of plasticizer (TEC) calculated using the Hertz and Oyen & Cook models. The elastic modulus of skin [28], determined under similar indentation conditions, is shown as a horizontal line for comparison with the standard deviation shown in grey. The data shown are the means and standard deviations determined from three different samples of each film and a minimum of eight indents per sample.

5. Conclusion

AFM and Raman spectroscopy have elicited information on the topography, elastic moduli and chemical distribution of polymeric films intended for dermal drug delivery. Raman mapping showed that the plasticizer (TEC) and model topical drug (BMV) were distributed homogenously throughout

both Eudragit and Klucel films. AFM images provided a nanoscale picture of the topography of the films. Nanoindentation of the films revealed that the elastic modulus decreased with increasing plasticizer content. The elastic moduli of films incorporating 20% and 40% w/w TEC bracketed that of human skin, suggesting that their flexibility and intimate contact *in situ* may be simply optimised. The derivation of a model for the extraction of the films' elastic moduli from AFM nanoindentation has facilitated the comparison of the films and the skin.

Further AFM and Raman microscopy investigations of these films will assess film formation on skin. The moisture from the skin may influence the films' mechanical properties. Raman chemical mapping of the films on the surface of the skin would reveal whether the distribution of the films' components changes after their initial formation as a function of the surface structure of the skin.

Acknowledgements

We thank John Mitchels, Sarah Cordery and Ashley Brewer for advice on various technical and practical aspects of the research described. We are grateful to Leo Pharma A/S and the University of Bath for financial support of the project.

References

1. Schroeder, I. Z.; Franke, P.; Schaefer, U. F.; Lehr, C. M. Development and characterization of film forming polymeric solutions for skin drug delivery. *Eur J Pharm Biopharm* **2007,** *65*, (1), 111-121.

2. Felton, L. A.; Porter, S. C. An update on pharmaceutical film coating for drug delivery. *Expert Opin Drug Del* **2013,** *10*, (4), 421-435.

3. Hall, L. T.; Bailes, J. E. Using Dermabond for wound closure in lumbar and cervical neurosurgical procedures. *Neurosurgery* **2005,** *56*, (1 Suppl), 147-50; discussion 147-50.

4. Ritterband, D. C.; Meskin, S. W.; Shapiro, D. E.; Kusmierczyk, J.; Seedor, J. A.; Koplin, R. S. Laboratory model of tissue adhesive (2-octyl cyanoacrylate) in sealing clear corneal cataract wounds. *Am J Ophthalmol* **2005,** *140*, (6), 1039-1043.

5. Jeng, D. K. A new, water-resistant, film-forming, 30-second, one-step application iodophor preoperative skin preparation. *Am J Infect Control* **2001,** *29*, (6), 370-376.

6. Evonik Industries, EUDRAGIT® application guidelines. 12 ed.; 2012.

7. Hercules Incorporated: Aqualon Division, Klucel® hydroxypropylcellulose - Physical and chemical properties 2001.

8. Frederiksen, K.; Guy, R. H.; Petersson, K. Formulation considerations in the design of topical, polymeric film-forming systems for sustained drug delivery to the skin. *Eur J Pharm Biopharm*. Submitted for publication, revised manuscript following "minor corrections" under consideration.

9. U.S. Food and Drug Administration - Center for Drug Evaluation and Research Inactive Ingredient Search for Approved Drug Products. http://www.accessdata.fda.gov/scripts/cder/iig/index.cfm (15th December 2014),

10. Lin, S. Y.; Lee, C. J.; Lin, Y. Y. Drug-Polymer Interaction Affecting the Mechanical-Properties, Adhesion Strength and Release Kinetics of Piroxicam-Loaded Eudragit-E Films Plasticized with Different Plasticizers. *J Control Release* **1995,** *33*, (3), 375-381.
11. Lecomte, F.; Siepmann, J.; Walther, M.; MacRae, R. J.; Bodmeier, R. Polymer blends used for the aqueous coating of solid dosage forms: importance of the type of plasticizer. *J Control Release* **2004,** *99*, (1), 1-13.
12. Bajdik, J.; Regdon, G.; Marek, T.; Eros, I.; Suvegh, K.; Pintye-Hodi, K. The effect of the solvent on the film-forming parameters of hydroxypropyl-cellulose. *Int J Pharm* **2005,** *301*, (1-2), 192-198.
13. Luppi, B.; Bigucci, F.; Baldini, M.; Abruzzo, A.; Cerchiara, T.; Corace, G.; Zecchi, V. Hydroxypropylmethylcellulose films for prolonged delivery of the antipsychotic drug chlorpromazine. *J Pharm Pharmacol* **2010,** *62*, (3), 303-309.
14. Cilurzo, F.; Gennari, C. G. M.; Minghetti, P. Adhesive properties: a critical issue in transdermal patch development. *Expert Opin Drug Del* **2012,** *9*, (1), 33-45.
15. Ebenstein, D. M.; Pruitt, L. A. Nanoindentation of biological materials. *Nano Today* **2006,** *1*, (3), 26-33.
16. Masterson, V. M.; Cao, X. P. Evaluating particle hardness of pharmaceutical solids using AFM nanoindentation. *Int J Pharm* **2008,** *362*, (1-2), 163-171.
17. Liao, X. M.; Wiedmann, T. S. Measurement of process-dependent material properties of pharmaceutical solids by nanoindentation. *J Pharm Sci-Us* **2005,** *94*, (1), 79-92.
18. Bhushan, B.; Tang, W.; Ge, S. Nanomechanical characterization of skin and skin cream. *J Microsc-Oxford* **2010,** *240*, (2), 135-144.
19. Bugay, D. E. Characterization of the solid-state: spectroscopic techniques. *Adv Drug Deliver Rev* **2001,** *48*, (1), 43-65.
20. Lin, W. Q.; Jiang, J. H.; Yang, H. F.; Ozaki, Y.; Shen, G. L.; Yu, R. Q. Characterization of chloramphenicol palmitate drug polymorphs by Raman mapping with multivariate image segmentation using a spatial directed agglomeration clustering method. *Anal Chem* **2006,** *78*, (17), 6003-6011.
21. Sasic, S.; Clark, D. A. Defining a strategy for chemical imaging of industrial pharmaceutical samples on Raman line-mapping and global illumination instruments. *Appl Spectrosc* **2006,** *60*, (5), 494-502.
22. Sasic, S.; Clark, D. A.; Mitchell, J. C.; Snowden, M. J. Analyzing Raman maps of pharmaceutical products by sample-sample two-dimensional correlation. *Appl Spectrosc* **2005,** *59*, (5), 630-638.
23. Sakamoto, T.; Matsubara, T.; Sasakura, D.; Takada, Y.; Fujimaki, Y.; Aida, K.; Miura, T.; Terahara, T.; Higo, N.; Kawanishi, T.; Hiyama, Y. Chemical mapping of tulobuterol in transdermal tapes using Microscopic Laser Raman Spectroscopy. *Pharmazie* **2009,** *64*, (3), 166-171.

24. Lunter, D.; Daniels, R. In vitro Skin Permeation and Penetration of Nonivamide from Novel Film-Forming Emulsions. *Skin Pharmacol Phys* **2013,** *26*, (3), 139-146.

25. Doub, W. H.; Adams, W. P.; Spencer, J. A.; Buhse, L. F.; Nelson, M. P.; Treado, P. J. Raman chemical imaging for ingredient-specific particle size characterization of aqueous suspension nasal spray formulations: A progress report. *Pharmaceut Res* **2007,** *24*, (5), 934-945.

26. Belsey, N. A.; Garrett, N. L.; Contreras-Rojas, L. R.; Pickup-Gerlaugh, A. J.; Price, G. J.; Moger, J.; Guy, R. H. Evaluation of drug delivery to intact and porated skin by coherent Raman scattering and fluorescence microscopies. *J Control Release* **2014,** *174*, 37-42.

27. Saar, B. G.; Contreras-Rojas, L. R.; Xie, X. S.; Guy, R. H. Imaging Drug Delivery to Skin with Stimulated Raman Scattering Microscopy. *Mol Pharmaceut* **2011,** *8*, (3), 969-975.

28. Beard, J. D.; Guy, R. H.; Gordeev, S. N. Mechanical tomography of human corneocytes with a nanoneedle. *Journal of Investigative Dermatology* **2013,** *133*, 1565-1571.

29. Sader, J. E.; Chon, J. W. M.; Mulvaney, P. Calibration of rectangular atomic force microscope cantilevers. *Rev Sci Instrum* **1999,** *70*, (10), 3967-3969.

30. Beard, J. D.; Burbridge, D. J.; Moskalenko, A. V.; Dudko, O.; Yarova, P. L.; Smirnov, S. V.; Gordeev, S. N. An atomic force microscope nanoscalpel for nanolithography and biological applications. *Nanotechnology* **2009,** *20*, (44).

31. Field, J. S.; Swain, M. V. A Simple Predictive Model for Spherical Indentation. *J Mater Res* **1993,** *8*, (2), 297-306.

32. Oyen, M. L.; Cook, R. F. Load-displacement behavior during sharp indentation of viscous-elastic-plastic materials. *J Mater Res* **2003,** *18*, (1), 139-150.

33. Lauer, M. E.; Siam, M.; Tardio, J.; Page, S.; Kindt, J. H.; Grassmann, O. Rapid Assessment of Homogeneity and Stability of Amorphous Solid Dispersions by Atomic Force Microscopy-From Bench to Batch. *Pharmaceut Res* **2013,** *30*, (8), 2010-2022.

34. Neumann, T., Determining the elastic modulus of biological samples using atomic force microscopy. JPK Instruments Application Report: pp 1-9.

35. Plassard, C.; Lesniewska, E.; Pochard, I.; Nonat, A. Investigation of the surface structure and elastic properties of calcium silicate hydrates at the nanoscale. *Ultramicroscopy* **2004,** *100*, (3-4), 331-338.

36. Weisenhorn, A. L.; Kasas, S.; Solletti, J. M.; Khorsandi, M.; Gotzos, V.; Romer, D. U.; Lorenzi, G. P. Deformation Observed on Soft Surfaces with an Afm. *P Soc Photo-Opt Ins* **1993,** *1855*, 26-34.

37. Beard, J. D.; Gordeev, S. N. Large flexibility of high aspect ratio carbon nanostructures fabricated by electron-beam-induced deposition. *Nanotechnology* **2010,** *21*, (47).

38. Geerligs, M.; van Breemen, L.; Peters, G.; Ackermans, P.; Baaijens, F.; Oomens, C. In vitro indentation to determine the mechanical properties of epidermis. *J Biomech* **2011,** *44*, (6), 1176-1181.

For Table of Contents Use Only

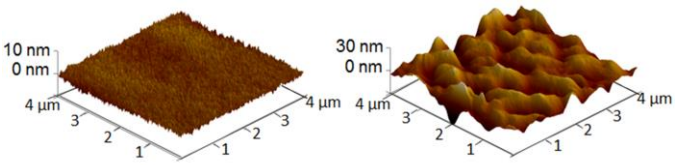

Characterisation of topical film-forming systems using atomic force microscopy and Raman micro-spectroscopy

Hazel Garvie-Cook[1,2], Kit Frederiksen[2,3], Karsten Petersson[3], Richard Guy[2], Sergey Gordeev[1]

1. Department of Physics, University of Bath, Bath, UK
2. Department of Pharmacy & Pharmacology, University of Bath, Bath, UK
3. LEO Pharma A/S, DK-250 Ballerup, Denmark